Delft University of Technology

A monolithic compliant large-range gravity balancer

Radaelli, G.; Herder, J. L.

Important note
To cite this publication, please use the final published version (if applicable).
Please check the document version above.

A monolithic compliant large-range gravity balancer

G. Radaelli[a,b], J.L. Herder[a]

[a] *Dept. Precision and Microsystems Engineering, Delft University of Technology, Delft, The Netherlands*
[b] *Laevo BV, Molengraaffsingel 12-14, Delft, The Netherlands*

Abstract

A new monolithic fully compliant gravity balancer is designed with help of a design approach based on shape optimization. The balancer consists of one single clamped-clamped complex-shaped beam on which a weight is attached. The beam is modeled as a planar isogeometric Bernoulli beam. The goal function of the optimization consists of an energy based evaluation of the load path of the beam which is compared with a desired response. The best result of the shape optimization has been constructed out of polycarbonate sheet and out of glass-fiber reinforced plastic laminate. Both have been tested on a compression test bench. The theoretical model has good resemblance with the experimental results.

Keywords: compliant mechanisms, static balancing, constant force generator

1. Introduction

Compliant mechanisms, i.e. mechanisms that achieve their motion from the deflection of their members instead of from kinematic constraints [1], are more challenging to design due to their inherent coupling between kinetics and kinematics. Since forces and deflection in these mechanisms can never be considered separately because of the flexibility of the members, the design methods for conventional rigid-body mechanisms cannot be directly applied. Alternative design methods have been developed over the past decades, and a majority of designers have found their way to lumped parameter models

---

like, e.g. pseudo-rigid-body models (PRBM) [2] [3] [4], in order to deal with these challenges, but compromising in terms of accuracy, freedom of shape, and moreover often basing their designs on equivalent rigid body mechanism designs.

Statically balanced compliant mechanisms (SBCM) [5] [6] are a subset of compliant mechanisms where undesired forces are counteracted by elastic forces generated by the deflection of the mechanism. These undesired forces can come from, e.g., an external payload [7] or stiffness, the self-weight of the system or an intrinsic stiffness[8] [9]. These forces are undesired since they either require more energy for actuation, they disturb a force signal to be transmitted, e.g., to provide haptic sense in surgical tools [10], or they result in higher stiffness and eigenfrequencies. Balancing these compliant mechanisms is thus an option to improve efficiency, force feedback fidelity, vibration isolation and energy harvesting properties.

In these and other types of mechanisms it is often desirable to follow a required force-displacement path with good accuracy in order to enhance the quality of balancing and thus its performance. Examples where following a force displacement path is relevant can be found in [11] [12] [13] [14].

Apart from balancing a weight, there are more applications of compliant constant force balancers. Examples include force regulation [15][16], overload protection [16], constant force actuators [17] and adaptive robot end-effector operations [18].

Recently a design approach has been proposed by the authors [19] that enables the design of compliant mechanisms with prescribed load-paths with good accuracy and great flexibility of shape. The method is based on shape optimization of elastic structures undergoing large deflections modeled through the isogeometric analysis (IGA) framework [20]. This is an emerging framework allied to the finite element method (FEM), but with increased accuracy and efficiency especially due to the absence of a conversion step between CAD geometry and analysis geometry.

The goal of this paper is to present a special design result. The design has been generated through the use of shape optimization and validated by the construction and measurements of physical models. The purpose of this design is to balance a weight, or constant force, over a fairly large vertical displacement without restricting the horizontal motion of the weight. The model consists of a fully distributed and monolithic compliant mechanism, that consists of a single branch prismatic beam.

The paper also presents the measurement setup, where the challenge is

to apply and to measure a vertical force while the motions in horizontal directions are not restrained.

Section 2 of this paper shows the formulation of the design problem, the model and details of the optimization. In section 3 the design resulting from the optimization is shown. Section 4 illustrates the design of the measurement setup and section 5 shows the measurement results. Respectively, sections 6 and 7 contain the discussion and conclusion.

2. Method

The current section describes the formulation of the design problem and discusses some inputs for the design optimization.

2.1. Problem statement

The goal of the design procedure is to find a compliant mechanism of which a selected point L is displaced downwards resulting in a constant vertical force upward over a given range. Consequently, this constant force can be replaced by a weight obtaining a statically balanced system.
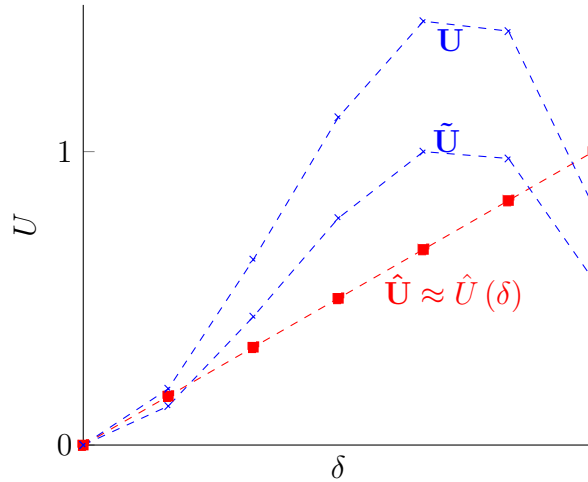
Figure 1: Linear reference energy $\hat{\mathbf{U}} \approx \hat{U}(\delta)$, energy obtained by computational model $\mathbf{U}$ and normalized obtained energy $\tilde{\mathbf{U}}$.

Considering a quasi-static and conservative mechanical system, a constant force mechanism is one that possesses a linearly increasing potential energy $\hat{U}(\delta)$ with respect to the vertical displacement δ at the point of application of the force and in its direction. This energy is evaluated at a

3

discrete amount of displacements yielding the array $\hat{\mathbf{U}}$. This reference array is defined as a linearly increasing sequence from zero to one as

$$\hat{U}_k = \frac{k-1}{m-1} \quad \text{for} \quad k = 1..m. \tag{1}$$

The array of potential energy obtained by the computational model $\mathbf{U}$ is defined as

$$\mathbf{U} = \begin{bmatrix} U_1(\delta_1) & U_2(\delta_2) & ... & U_m(\delta_m) \end{bmatrix} \tag{2}$$

where U_k are the values of the potential energy of the system in an equilibrium situation corresponding to the applied displacement δ_k at step k. In this case δ_k, $k = 1..m$ is a discrete set of linearly spaced vertical displacements of the selected point.

Since the sizing (thickness, width, etc.,) of the resulting design has a direct relation to the magnitude of the constant force to be balanced, i.e. the payload, and less influence on the development of the force, the goal function will be made independent of the amplitude by normalization. This is done by normalizing the array of obtained energy values $\mathbf{U}$ so that the minimum value corresponds to zero and the maximum value corresponds to one. The norm energy array is obtained by scaling every entry of $\mathbf{U}$ according to

$$\tilde{U}_k = \frac{U_k - U_{min}}{U_{max} - U_{min}} \quad \text{for} \quad k = 1..m. \tag{3}$$

As such, the goal function to be optimized is formulated as

$$f_0 = \frac{\left(\tilde{\mathbf{U}} - \hat{\mathbf{U}}\right)\left(\tilde{\mathbf{U}} - \hat{\mathbf{U}}\right)^T}{\hat{\mathbf{U}}\hat{\mathbf{U}}^T} \tag{4}$$

which is the normalized sum of squared errors between reference energy array $\hat{\mathbf{U}}$ and the normalized obtained energy $\tilde{\mathbf{U}}$.

There is an initial build up of the vertical force expected since the system starts from rest and goes to a higher force level. This build up is desired to be short and steep, to keep the constant force region as large as possible. In terms of energy this means that the slope goes from initially zero to a certain slope which from that point on is desired to be kept constant. These initial steps of build-up influence the goal function negatively and are therefore omitted in above expressions. The precise amount of steps to be omitted is a design choice.

The mechanical model that has been used is that of a single beam clamped at the two endpoints. The beam is modeled by an isogeometric, geometrically nonlinear Bernoulli beam [21], with a linear material constitutive law, of which the potential energy is evaluated at every imposed boundary condition. With the first material, polycarbonate (PC), that will be used in the experiments (section 4) a discrepancy is expected because of the material nonlinearity. For the second one, glass-fiber reinforced plastic (GFRP), this model is suitable because the majority of fibers are placed longitudinally with respect to the beam. It will be validated experimentally that a 1D planar beam model gives accurate enough results.

In the isogeometric formulation, a B-spline with relatively small amount of control points $\mathbf{B}_i$, with $i = 1..n$, describes the geometry of the beam, see Fig. 2. Consequently, for analysis, the shape is refined in a B-spline with a larger amount of control points $\mathbf{P}_j$, with $j = 1..r$ and $r >> n$, where the displacements of the control points represent the degrees of freedom of the system.
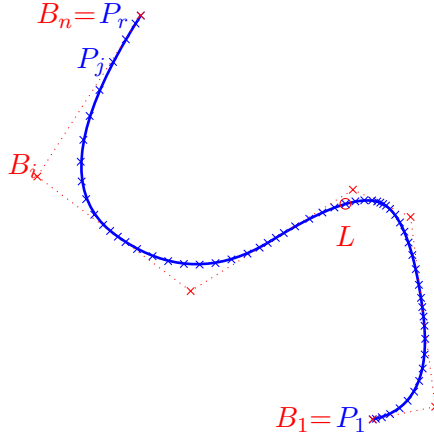

Figure 2: B-spline with original control points $\mathbf{B}_i$, with $i = 1..n$, refined control points $\mathbf{P}_j$, with $j = 1..r$, and point of displacement application L.

The vertical displacement is applied at the central control point of the refined B-spline, point L. Strictly taken, this is not the same as applying a displacement on a point on the curve itself, since the B-spline is generally not interpolatory, i.e. the curve generally does not intersect the control points.

However, the offset between control points and curve becomes smaller as the number of control points increases. In the presented analysis the shape is determined by $n = 7$ control points and is refined to $r = 50$ control points. The distance between the curve and point L is less then $0.1mm$ on a $300mm$ scale model. This is small compared with, e.g., fabrication and other errors.

Furthermore the curve is defined by the open, uniform knot vector $\Xi = \begin{bmatrix} 0 & 0 & 0 & 0.2 & 0.4 & 0.6 & 0.8 & 1 & 1 & 1 \end{bmatrix}$

2.3. Shape optimization
2.3.1. Optimization parameters

The set of control points $\mathbf{B}$ are the parameters of the optimization. For convenience in the applications of bounds for the optimization and interpretation of the results, the positions of the control points are re-parameterized according to

$$\mathbf{B} = \begin{bmatrix} B_{1_x} \\ B_{1_y} \\ B_{2_x} \\ B_{2_y} \\ B_{3_x} \\ B_{3_y} \\ B_{4_x} \\ B_{4_y} \\ \vdots \end{bmatrix} = \begin{bmatrix} q_1 \\ q_2 \\ q_1 + q_3 c\,(q_4) \\ q_2 + q_3 s\,(q_4) \\ q_1 + q_3 c\,(q_4) + q_5 c\,(q_4 + q_6) \\ q_2 + q_3 s\,(q_4) + q_5 s\,(q_4 + q_6) \\ q_1 + \ldots + q_7 c\,(q_4 + q_6 + q_8) \\ q_2 + \ldots + q_7 s\,(q_4 + q_6 + q_8) \\ \vdots \end{bmatrix} \tag{5}$$

where c and s are the shorthand notations for cos and sin, and $\mathbf{q}$ defined as

$$\mathbf{q} = \begin{bmatrix} B_{1_x} & B_{1_y} & l_1 & \theta_1 & l_2 & \theta_2 & l_3 & \theta_3 & \ldots \end{bmatrix}. \tag{6}$$

This transforms the parameters of optimization from an array of Cartesian coordinates to a sequence of lengths l_k and relative angles θ_k, i.e. it describes the control polygon of the spline as if it were a linkage chain, see Fig. 3. By this transformation it becomes easy to apply limits to the search space. For example, limiting the angles avoids sharp corners in the beam. Additionally giving a lower limit to the lengths also helps avoiding loops of the spline which in practice leads to unfeasible structures.

The applied optimization bounds on the lengths of the sides of the control polygon are $[0.05 \leq l \leq 0.15]$ and their relative angles $[-2 \leq \theta \leq 2]$. The total vertical applied displacement is $0.21\ [m]$.
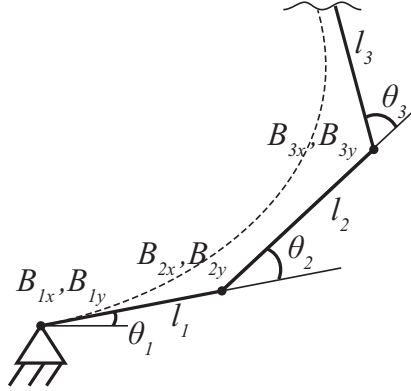
6

Figure 3: Transformation of coordinates of the control points in a set of generalized coordinates, described by the lengths and angles of the links of a linkage chain, representing the control polygon.

In the current optimization a control polygon of 7 control points is used. The first two parameters of vector $\mathbf{q}$, i.e. the position of the begin of the beam, are fixed to zero. In this particular case these parameters only determine the global position of the mechanism in space and have no influence on its behavior. This results in 12 optimization parameters of which 6 are the lengths of the control polygon sides and 6 are their relative angles.

2.3.2. Sizing parameters

The optimization is performed on the shape parameters only, while sizing parameters are kept out of consideration by normalizing for an undetermined payload, as discussed. As soon as the shape is found it is possible to change the sizing variables, i.e. the cross-section dimensions and the Young's modulus, to match a desired payload. As long as the Euler-Bernoulli conditions, i.e. *length >> thickness*, are met, the sizing will not influence the balancing results significantly. Eventually, an additional optimization run can restore an altered behavior due to sizing changes.

The dimensions and properties used as starting point in current optimization run are given in table 1, meant for a glass fiber reinforced plastic slender beam construction.

2.3.3. Algorithm

The selected optimization algorithm is the Sequential Quadratic Programming (SQP) from the Matlab® *Optimization Toolbox*, started at 50 different starting points randomly distributed over the search space using

parameter	value	unit
E	25	$[GPa]$
width	0.15	$[m]$
thickness	0.002	$[m]$

Table 1: Material and sizing parameters

the *MultiStart* option in the *Global Optimization Toolbox*.

3. Optimization results

Out of the 50 runs from different random starting points the best result has been selected. For this run the converged solution $\mathbf{q}_{end}$ is shown in table 2. The behavior of the optimized geometry is shown in Fig. 4, showing the undeformed geometry in red (thick line) and the deformed geometries corresponding to every displacement step in blue (thin lines). The red crosses are the control points of the design vector and the red circle is the point of application of the vertical displacement. Figure 5 shows the optimized energy graph (blue circled) compared to the reference energy (red crossed). Since the difference between the obtained and reference energy is hardly visible, the error between both is plotted in Fig. 6. The final objective function, i.e. the normalized sum of squared errors, is $1.48e - 4$. The resulting reaction force in vertical direction due to the applied displacement is plotted in Fig. 7. Finally an overview of the strains is provided in Fig. 8. Here for every load step the strain is shown for the innermost material layer (green) and the outermost layer (blue). On the horizontal axis the parameter of the b-spline is ξ which ranges from 0 to 1 from the begin to the end of the curve.

4. Experimental evaluation

The construction of the physical model is shortly presented and the measurement setup explained.

par.	unit	$\mathbf{q}_{end}$
B_{1_x}	$[mm]$	0.00
B_{1_y}	$[mm]$	0.00
l_1	$[mm]$	85.8
θ_1	$[rad]$	1.23
l_2	$[mm]$	10.8
θ_2	$[rad]$	0.06
l_3	$[mm]$	12.6
θ_3	$[rad]$	1.54
l_4	$[mm]$	05.1
θ_4	$[rad]$	0.73
l_5	$[mm]$	12.9
θ_5	$[rad]$	1.24
l_6	$[mm]$	11.9
θ_6	$[rad]$	0.01

Table 2: Optimized design vector $\mathbf{q}_{end}$

4.1. Prototype construction

As a preliminary investigation before making a glass-fiber reinforced plastic (GFRP) version of the beam, as foreseen in the optimization material parameters, a polycarbonate version of the same beam is constructed. Poly-carbonate is broadly available, cheap and has fairly good mechanical properties. Moreover the production process is fairly simple and leads quickly to acceptable results. Two beams have been constructed with different plate thicknesses: 1 mm and 2 mm. A one-sided mould is CNC-milled out of high-density foam material, see Fig. 9. A polycarbonate plate is heated above its glass-transition temperature and then draped onto the mould. When the plastic reaches ambient temperature again, the beam is ready to be clamped onto the supporting structure, see Fig. 10.

After, using the same type of mould, the same shape is fabricated out of glass-fiber reinforced plastic (GFRP), which is epoxy in this case. This is done using a vacuum infusion process. The dry fibers are placed onto the mould and sealed with a vacuum bag. Then the vacuum causes the liquid resin to infuse and spread through all fibers. The resin is then cured in an oven to get optimal strength. The resulting shapes are shown in Fig. 11. Multiple layups have been constructed. The two presented in this work have the laminate layups [0 -45/45 0] and [0 -45/45 0 -45/45 0] , where the fibers in the 0-direction are unidirectional fibers (UD) of S2-type
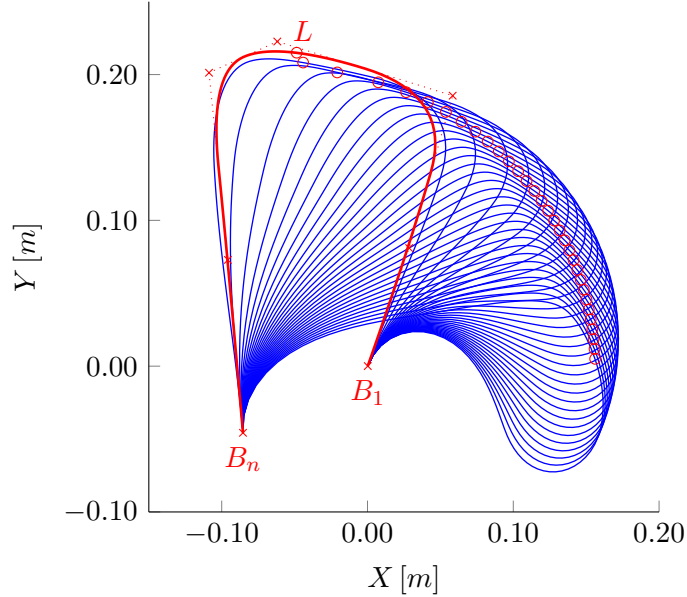
Figure 4: Undeformed geometry of the optimized shape (red) and deformed geometries corresponding to every displacement step (blue). The red dot indicates the point of application of the vertical displacement L.

glass and the ones in $-45/45$-directions are woven fibers of E-type glass. The UD S2-glass layers have a thickness of $0.2\ mm$, the woven E-glass have a thickness of $0.06\ mm$ for each layer. The S2-type glass is selected because of the superior stiffness and strength properties. The woven E-glass fibers are applied to prevent easy crack propagation in longitudinal direction, but have a minor influence on the bending properties. This justifies the use of a 1D planar element, i.e. a beam element, with respect to a more complex orthotropic shell element.

4.2. Measurement setup

For the experimental evaluation the vertical reaction force is measured while a displacement is applied at the selected point. It is important that only a vertical displacement is applied, while the horizontal motion of that point is completely free. This is a challenge for conventional compression testing machines that travel along a straight line. To overcome this limitation, the base of the compliant mechanism is placed on a planar horizontal stage. This stage consists of three sets of orthogonally placed rollers that affect the planar translations with low friction. As shown in Fig. 12 two long steel rollers are placed in parallel with the direction of motion of the
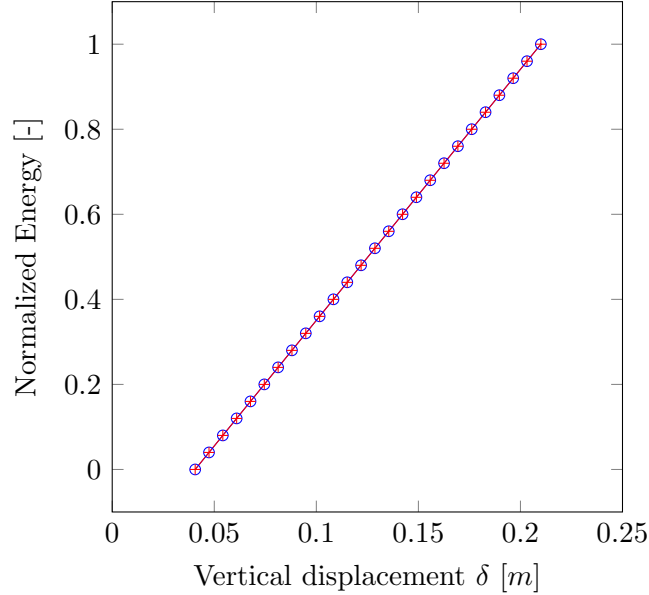
Figure 5: Optimized energy graph $\tilde{\mathbf{U}}$(blue circled) and reference energy graph $\hat{\mathbf{U}}$ (red crossed).

support of the beam. Other two rollers are placed in the perpendicular direction on top of the first set of rollers. Again other two rollers are placed in the direction of motion right underneath the support base of the beam. The roller configuration is chosen such that only point contacts are made between rolling parts and that the reaction force is always within the support polygon of these point contacts. The only motion in the horizontal plane that is restricted is the rotation. However, no such rotational motion is expected in this design, and no such tendency was observed during the measurements.

The interface between the beam and the load cell has been designed such that the applied displacement is evenly distributed along a line corresponding to the selected point in the planar representation of the beam. This has been achieved by a knife-edge bearing, created by a rectangular prismatic aluminum bar that makes contact with the beam only at one lower corner, see Fig. 13. This contact is maintained during the whole range of motion. The position of the contact line on the beam is maintained by a double-sided adhesive tape that sticks to the beam on one side of the contact line and sticks to the bar at the other side of the line, see an impression in Fig.
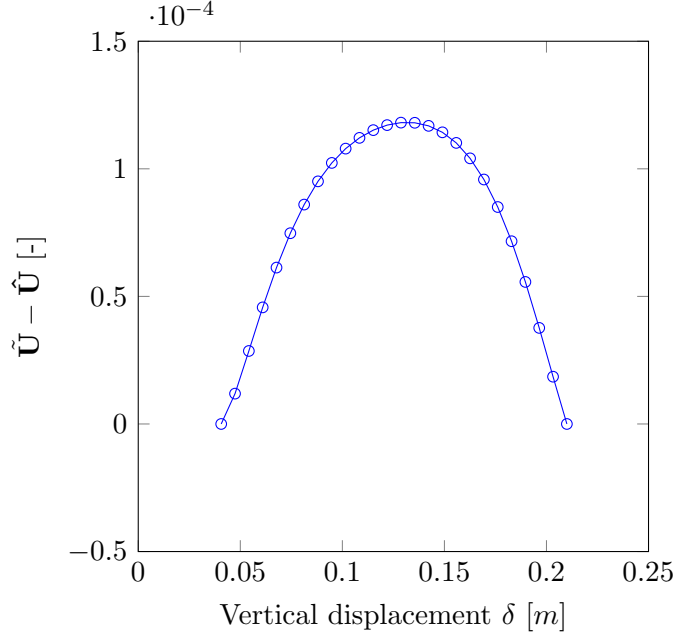
11

Figure 6: Error between optimized energy $\tilde{\mathbf{U}}$ and reference energy $\hat{\mathbf{U}}$.

14. The tape is loaded in tension throughout the whole motion, therefore a fiber-reinforced tape is very suitable.

5. Measurement results

The results of the force measurements are shown in Fig. 15 for the polycarbonate version. The higher blue line is the force measured with the 2 mm plate in a forward and backward motion cycle. The lower blue line is the force measured on the 1 mm plate. Figure 16 shows the results from the GFRP version. The lower line represents the thinner laminate, which measures 0.7 mm on average, and the higher line represents the thicker laminate, which measures 0.9 mm on average. In red the theoretical forces from the computational model are plotted for comparison. The amplitude of these model forces are fitted onto the measured data because the exact cross-sectional properties are hard to predict, especially with the GFRP laminate. This circumvents the need to specifically tests these properties, which is out of the scope of this work and irrelevant for the outcome.

The fitting is done by using the thickness of the beam as a parameter and the coefficients of variation of the root mean squared error (CV(RMSE)) as a minimization criterion. The criterion is defined as
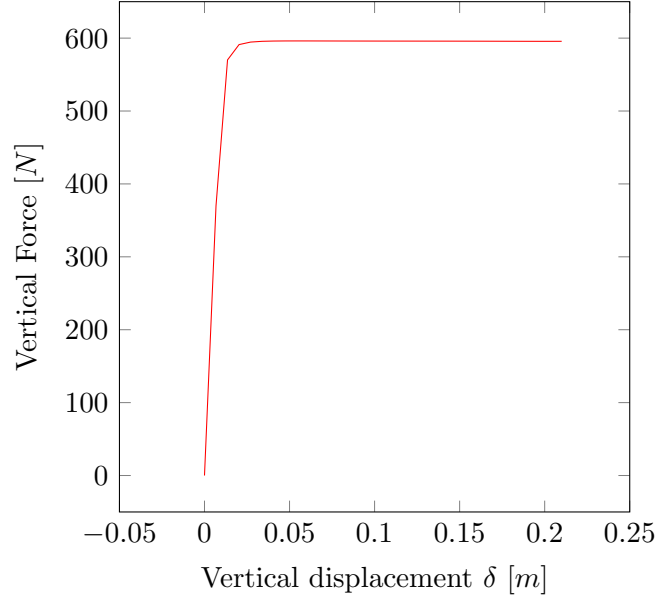
Figure 7: Optimized vertical force vs vertical displacement δ.

$$CV(RMSE) = \frac{RMSE}{\bar{y}} \tag{7}$$

where $RMSE$ is given by

$$RMSE = \sqrt{\frac{\sum_{t=1}^{n} (\hat{y}_t - y)^2}{n}}, \tag{8}$$

$\bar{y}$ is the mean of the measured values y and $\hat{y}$ represents the values predicted by the model. The range $t = 1..n$ for which this measure is calculated starts at the position for which the force is optimized, i.e. after the 6 steps of the ramp up. This corresponds to a displacement of 40 mm from the unloaded position.

Table 3 contains the CV(RMSE) for the four measured samples. This measure is chosen to make the results comparable despite of the different amplitude of the forces. The values are given for the upper line of the hysteresis loop corresponding to the forward part of the motion cycle.
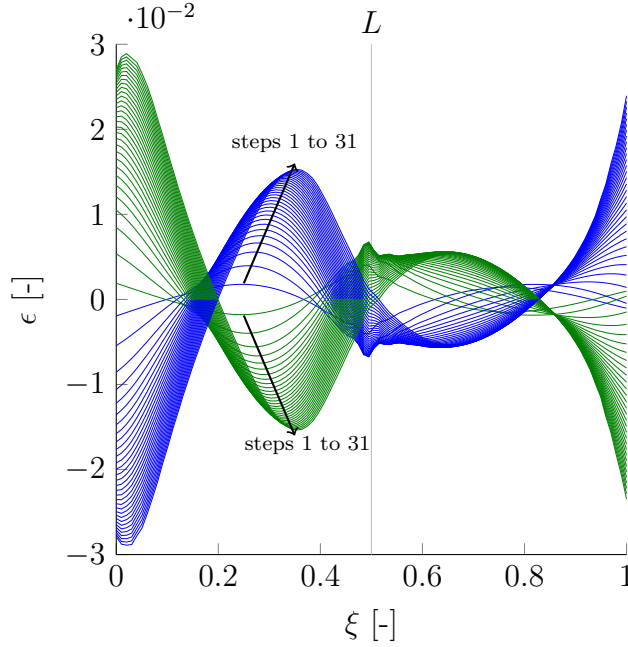
13

Figure 8: Material strains for a 2 *mm* thick plate. The lines represent the strain across the length of the beam, from curve parameter $\xi = 0$ to $\xi = 1$. The green lines represent the innermost material layer and the blue lines represent the outermost material layer. The lines are drawn for every load step from 1 to 31. Discontinuity can be observed at the position corresponding to point L, where the load is applied.

6. Discussion

6.1. Modeling and optimization

The optimization works well as design-aid for some special types of compliant mechanisms. The designed load-path, the goal of the optimization, is well achieved by this approach. It is not trivial that by virtue of the shape of the beam alone, such a near-perfect constant force can be generated by this elastic system.

Interesting to point out is the self searching behavior of the point of application of the payload in horizontal direction. In fact this point does not need to be constrained over a particular path in order to achieve the desired behavior. The point moves vertically by imposing the displacement but at every vertical step it finds the horizontal position of minimal energy for the system.

Even though the goal function of the optimization is known to be non-convex, thus not guaranteeing convergence to a global optimum, by use

14

Figure 9: One sided mould out of high-density foam material.

Sample	1 mm PC	2 mm PC	0.7 mm GFRP	0.9 mm GFRP
$CV\,(RMSE)$	0.0287	0.0046	0.0087	0.0032

Table 3: Coefficients of variation of root mean squared error CV(RMSE) values for all measured samples with respect to the modeled force

of a multi-start method enough satisfying local minima have been found. It must be noted that for this situation it is not important to find the global minimum as long as the value of the local minimum is small enough in a practical sense. Since the goal function, by its definition, is lower-bounded at zero, finding the absolute zero is not better than finding a sufficiently small objective value. The threshold of good enough is of course a subjective matter and depends on the design requirements. Consider that the effect of a slightly higher goal function will in practice be overshadowed by imperfections of the physical system.

On the other hand it must be considered that due to the presence of many local optima, it always remains unclear which minima were *not* found by the optimization. Did it miss some interesting, better, more efficient solutions? One where with less material a higher payload is balanced? Or
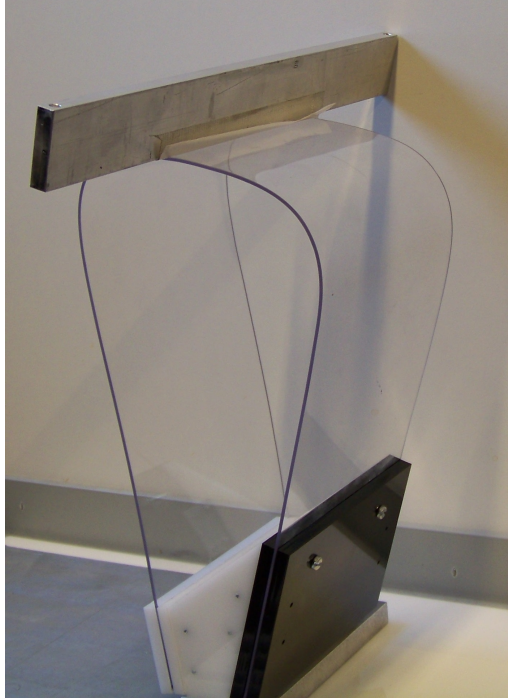
Figure 10: Polycarbonate beam clamped onto support structure.

one where the stresses in the material are distributed more evenly? These questions are subjects of investigation which may lead to improved designs and procedures in future.

One aspect of the modeling that is known to produce an error is the offset from the control point on which the displacement is applied, with respect to the beam surface. However, in the resulting geometry and with the applied refinement this offset is in the order of a tenth of a millimeter. This is considered insignificant especially compared to the more significant manufacturing errors.

A choice made in the modeling steps is to remove the first few load-steps, in this case the first 5 out of 31. This is a deliberate choice of the designer that may influence the result to a large extend. The authors have chosen for a minimal amount, such that the ramp-up would be as steep as possible. Choosing a larger amount presumably simply results in good balancing properties but with a slower ramp-up and a relatively smaller range of motion. A smaller amount of steps has the risk that the first few steps that are not removed will influence the goal function too much in a
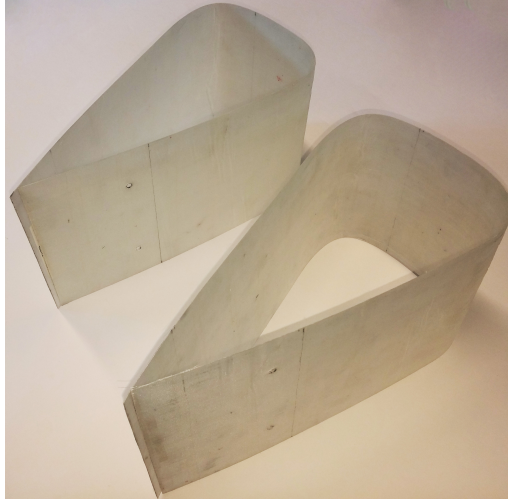
Figure 11: Glass-fiber reinforced plastic springs, manufactured by a vacuum infusion process.

negative sense, thus bringing the algorithm further away from potentially good results.

6.2. Prototype

In the physical models out of polycarbonate, it must be taken into consideration that this thermoplastic has a strongly nonlinear stress-strain characteristic. In the model however, a linear constitutive law has been adopted. Therefore an error in the measurements is to be expected that derives from this simplification. It can be observed that the 1 *mm* prototype seems to have a better match with the model, while the 2 *mm* prototype has a more rounded transition between the ramped part of the force and the constant part. This difference with the model, where the transition is clearly sharper, is considered to be related with nonlinearity of the material: The 2 *mm* version achieves higher strains and thus reaches further into the nonlinear stress-strain curve, while the 1 *mm* stays in the region where the stress-strain curve can be considered linear.

Furthermore, inaccuracies deriving from this particular production method must be taken into account. When the material sheet is cooling down it shrinks. This can result in a transverse curvature that has a significant effect on the cross-section geometry. In fact, a strip with a transverse curvature, e.g. a tape measure, has totally different stiffness behavior than a flat strip.
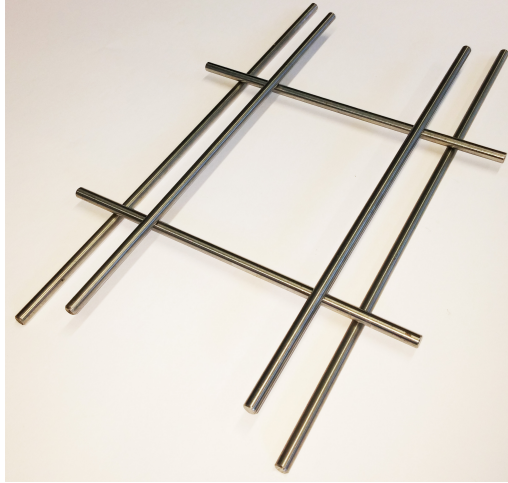
17

Figure 12: Rollers setup used as planar bearing underneath the beam support structure.

The manufacturing of the GFRP yields quite some uncertainties. Although manufactured by a trustworthy and experienced company, it is still a challenge with this method to have an uniformly distributed thickness. In fact there were two more springs manufactured ranging up to a thickness of 2 mm, which is the thickness used in the optimization run. Unfortunately those springs broke due to imperfections in the laminate.

Despite the manufacturing errors, the results of the measurements are still impressive. The output force in both cases is following a nice straight line and small deviations from the model.

6.3. Measurement

The measurement setup is simple and effective. It contains, except for the test bench, no particularly complex or expensive components. The support on rollers provides low friction and high vertical stiffness of the support. Also the taped rectangular bar making the line-contact with the polycarbonate plate performs properly.

It can be noted from the measured data that there is a significantly higher noise in the beginning of the constant-force range. Even though the normal force, and thus the load on the rollers, is nearly constant, the horizontal velocity of the base is significantly higher there and goes back to zero at the end of the range. As visible in Fig. 4, the point of application of the displacements almost describes an arc: horizontal at the start and vertical at the end. Also there is a sudden acceleration sideways at the

Figure 13: Knife-edge bearing for the application of a vertical motion along a line of the surface. Double-sided adhesive tape holds the corner of the aluminum bar on its place.

very beginning of the motion due to the buckling behavior of the structure. Both the oscillations of the structure and the imperfections in the rollers result in higher noise and oscillations under the described conditions of high acceleration and velocity.

Similar reasoning can explain the fact that the hysteresis in the measurement results is high in the beginning of the displacement and becomes smaller at the end of the range of motion, even though the vertical force does not change so much. At the begin the horizontal motion of the rollers is substantially larger than at the end where the rollers are almost standing still. Therefore there is more friction generated at the beginning and almost no friction generated at the end. The samples with higher normal force on the bearing setup (2 mm PC and 0.9 mm GFRP) have substantially higher friction losses, as expected.

7. Conclusion

This paper presents a new monolithic, compliant, single branch and prismatic cross-section beam that balances a large weight over a large stroke with virtually perfect accuracy in the model. Moreover the system is self-searching in horizontal direction, i.e the point of application of the weight does not have to be constrained over a certain path or line.
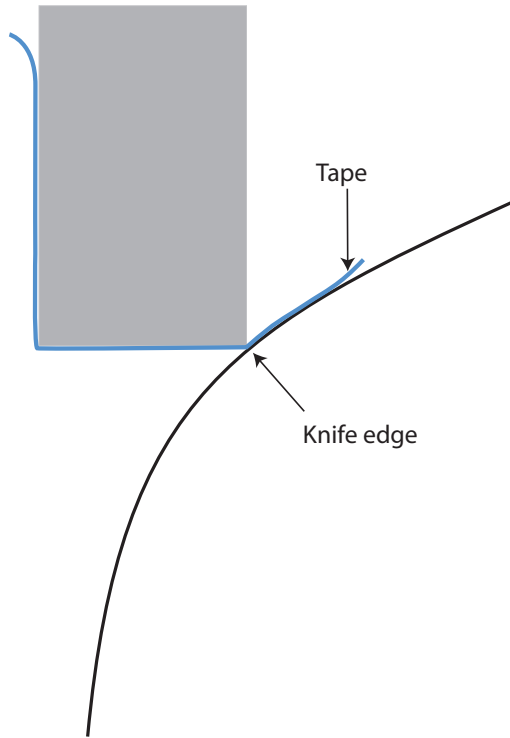
Figure 14: Schematic of the adhesive tape holding the knife-edge bearing on its place on the surface of the beam.

The previously presented design approach comprising a shape optimization procedure has been validated successfully by virtue of a non-trivial example. A rather complex shape was found that is able to exhibit a predefined complex behavior, i.e. large stroke with constant force. Such a design challenge is not easily achieved with existing methods for compliant mechanism design.

Physical models have been constructed for the validation of the results. A polycarbonate sheet has been thermoformed and draped onto a mould and GFRP laminate has been shaped onto the same mould.

The experimental validation of the numerical models shows a good resemblance between both. The observed errors can be explained by predictable causes. Especially the non-linearity of the material, the imperfection of the shape and the rollers are the main sources of errors.
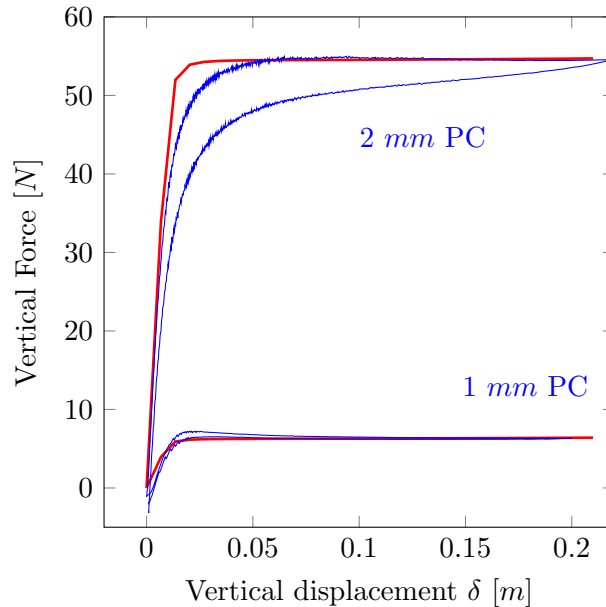
Figure 15: Comparison of vertical force from the measurements and the model for the polycarbonate model, both 1 mm and 2 mm thickness, in forward (up) and backward (under) direction.

Acknowledgment

[1] L. L. Howell, Compliant Mechanisms, John Wiley and Sons Inc., New York,US, 2001.

[2] L. L. Howell and A. Midha, A Method for the Design of Compliant Mechanisms With Small-Length Flexural Pivots, Journal of Mechanical Design 116 (1) (1994) 280–290. doi:10.1115/1.2919359.

[3] W. Nianfeng, L. Xiaohe, Z. Xianmin, Pseudo-rigid-body model for corrugated cantilever beam used in compliant mechanisms, Chinese Journal of Mechanical Engineering 27 (1) (2014) 122–129. doi:10.3901/CJME.2014.01.122.

[4] D. Bandopadhya, B. Bhattacharya, A. Dutta, Pseudo-rigid body modeling of IPMC for a partially compliant four-bar mechanism for work volume generation, Journal of Intelligent Material Systems and Structures 20 (1) (2009) 51–61. doi:10.1177/1045389X08088784.

[5] J. L. Herder, F. P. A. van den Berg, Statically balanced compliant mechanisms (SBCM's), an example and prospects, in: Proceedings ASME DETC 26th Biennial Mechanisms and Robotics Conference, 2000. doi:DETC2000/MECH-14144.

[6] S. Deepak R, Static balancing of rigid-body linkages and compliant mechanisms, PhD Thesis, Indian Institute of Science, Bangalore, India (May 2012).
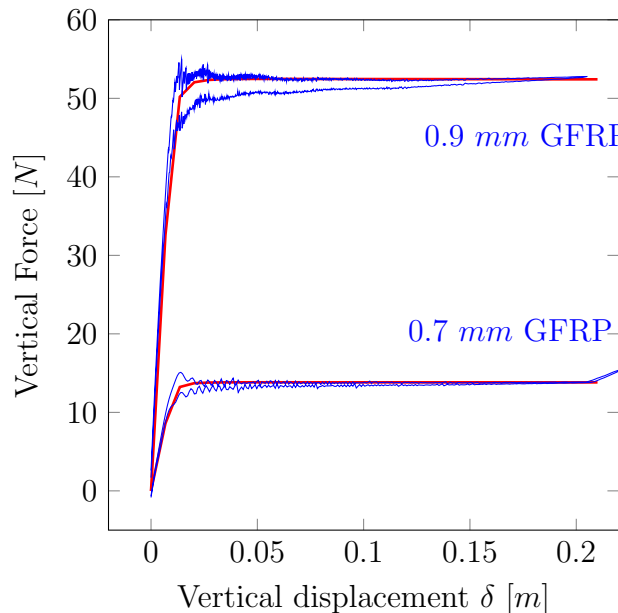
Figure 16: Comparison of vertical force from the measurements and the model for the GFRP model, both 0.7 *mm* and 0.9 *mm* thickness, in forward (up) and backward (under) direction.

[7] A. Dunning, N. Tolou, J. Herder, A compact low-stiffness six degrees of freedom compliant precision stage, Precision Engineering 37 (2) (2013) 380 – 388. doi:http://dx.doi.org/10.1016/j.precisioneng.2012.10.007.
URL http://www.sciencedirect.com/science/article/pii/S0141635912001729

[8] N. Tolou, J. A. Gallego, J. L. Herder, Statically balanced compliant micro mechanisms (sb-mems): A breakthrough in precision engineering, Mikroniek 50 (6) (2010) 20–25.

[9] K. Hoetmer, G. Woo, C. Kim, J. Herder, Negative stiffness building blocks for statically balanced compliant mechanisms: Design and testing, Journal of Mechanisms and Robotics 2 (4) (2010) 041007–1–7. doi:10.1115/1.4002247.
URL http://dx.doi.org/10.1115/1.4002247

[10] A. Stapel, J. L. Herder, Feasibility study of a fully compliant statically balanced laparoscopic grasper, ASME Conference Proceedings 2 (46954) (2004) 635–643. doi:10.1115/DETC2004-57242.
URL http://link.aip.org/link/abstract/ASMECP/v2004/i46954/p635/s1

[11] C. Vehar-Jutte, Generalized Synthesis Methodology of Nonlinear Springs for Predescribed Load-Displacement Functions, PhD Thesis, The University of Michigan, Michigan, USA (2008).

[12] L. C. Leishman, M. B. Colton, A pseudo-rigid-body model approach for the design of compliant mechanism springs for prescribed force-deflections, in: Proceedings of ASME IDETC/CIE 2011, 2011, pp. 93–102. doi:10.1115/DETC2011-47590.

[13] E. G. Merriam, S. Magleby, M. Colton, L. L. Howell, The design of a fully compliant statically balanced mechanism, in: Proceedings of ASME IDETC/CIE 2013, 2013.

[14] Ü. Sönmez, C. C. Tutum, A compliant bistable mechanism design incorporating elastica buckling beam theory and pseudo-rigid-body model, J. Mech. Des. 130 (4) (2008) 042304. doi:10.1115/1.2839009.

[15] D. Nahar, T. Sugar, Compliant constant-force mechanism with a variable output for micro/macro applications, in: Robotics and Automation, 2003. Proceedings. ICRA '03. IEEE International Conference on, Vol. 1, 2003, pp. 318–323 vol.1. doi:10.1109/ROBOT.2003.1241615.

[16] H.-T. Pham, D.-A. Wang, A constant-force bistable mechanism for force regulation and overload protection, Mechanism and Machine Theory 46 (7) (2011) 899 – 909. doi:http://dx.doi.org/10.1016/j.mechmachtheory.2011.02.008.
URL http://www.sciencedirect.com/science/article/pii/S0094114X11000425

[17] G. Berselli, R. Vertechy, G. Vassura, V. Parenti Castelli, Design of a single-acting constant-force actuator based on dielectric elastomers, J. Mechanisms and Robotics 1 (3) (2009) 031007.

[18] C.-C. Lan, J.-H. Wang, Y.-H. Chen, A compliant constant-force mechanism for adaptive robot end-effector operations, in: Robotics and Automation (ICRA), 2010 IEEE International Conference on, 2010, pp. 2131–2136. doi:10.1109/ROBOT.2010.5509928.

[19] G. Radaelli, J. L. Herder, Isogeometric shape optimization for compliant mechanisms with prescribed load paths, in: Proceedings ASME IDETC/CIE 2014, 2014. doi:DETC2014-35373.

[20] T. Hughes, J. Cottrell, Y. Bazilevs, Isogeometric analysis: Cad, finite elements, nurbs, exact geometry and mesh refinement, Computer Methods in Applied Mechanics and Engineering 194 (3941) (2005) 4135 – 4195.

[21] A. P. Nagy, Isogeometric Design Opitmization, PhD Thesis, Delft University of Technology, Delft, The Netherlands (December 2011).